An analytical study for nonlinear free and forced vibration of electrostatically actuated MEMS resonators

S.K. Lai[a,b,*], **X. Yang**[a], **C. Wang**[a], **W.J. Liu**[c,a]

[a] *Department of Civil and Environmental Engineering, The Hong Kong Polytechnic University, Hung Hom, Kowloon, Hong Kong, PR China*

[b] *The Hong Kong Polytechnic University Shenzhen Research Institute, Nanshan, Shenzhen, PR China*

[c] *School of Electro-Mechanical Engineering, Guangdong University of Technology, Guangzhou 510006, PR China*

Abstract

This work aims to construct accurate and simple lower-order analytical approximation solutions for the free and forced vibration of electrostatically actuated MEMS resonators, in which geometrical and material nonlinearities are induced from the mid-plane stretching, dynamic pull-in characteristics, electrostatic forces and even intrinsic properties. Due to the complexity of nonlinear MEMS systems, the quest of exact closed-form solutions for these problems is hardly obtained for parametric design and analysis, in particular for harmonically forced nonlinear systems. To examine the simplicity and effectiveness of the present analytical solutions, two illustrative cases are taken into consideration. First, the free vibration of a doubly-clamped microbeam suspended on an electrode due to a suddenly applied DC voltage is considered. Based on the Euler-Bernoulli beam theory and the von Karman type nonlinear kinematics, the dynamic motion of the microbeam is further discretized by the Galerkin method to an autonomous system with general nonlinearity, which can be solved analytically by using the Newton harmonic balance method. In addition to large-amplitude free vibration, the primary resonance response of a doubly-clamped microbeam driven by two symmetric electrodes is also investigated, where the microbeam is actuated by a bias DC voltage and a harmonic AC voltage. Following the same decomposition approach, the governing equation of a harmonically forced beam model can be transformed to a

[*]Corresponding author. *E-mail:* sk.lai@polyu.edu.hk

non-autonomous system with odd nonlinearity only. Then, analytical approximation solutions are derived to analyze the steady-state resonance response of such a problem under a combination of various DC and AC voltage effects. Finally, the analytical approximation results of both cases are validated and they are in good agreement with those obtained by the standard Runge-Kutta method.

Keywords: Analytical approximations, MEMS resonators, Nonlinear dynamics, Free and forced vibration, Primary resonance response.

1. Introduction

With the advancement of sensing and actuating technologies, micro-electro-mechanical systems (MEMS) have gained tremendous attention in a wide range of engineering applications, e.g., signal filtering technique, chemical and mass sensors, and probe-based microscopy.[1-3] This is mainly due to its superior properties of light weight, small size and low power consumption. In general, fully clamped microbeams are the major structural components in most MEMS resonators. Basically, there exist geometrical and material nonlinearities in electrically driven MEMS resonators caused by the mid-plane stretching, dynamic pull-in behavior, electrostatic force and material properties. Among various factors, electrostatic forces are the major parameter that is inversely proportional to the square of the distance between the microbeam and the actuated electrode in a MEMS resonator. Under strong external excitations, MEMS systems may undergo large-amplitude deformations, thereby inducing axial residue stress and damping effect.[4] Besides, the pull-in instability is also a common undesirable phenomenon in MEMS devices,[5-7] this is an actuation problem that can lead to strongly nonlinear dynamic behavior, namely a saddle-node bifurcation.[8] In order to determine the influence of geometrical and material nonlinearities on the performance of MEMS systems, it is highly desired to have a better understanding of the nonlinear dynamic behavior of such resonators, which is also useful for parametric design and analysis of advanced MEMS resonators in real-life engineering applications.

In the literature, many experimental and theoretical studies have been carried out to investigate the nonlinear dynamic behavior of microbeams.[9,10] In terms of theoretical analysis, a single-degree-of-freedom beam model is normally adopted to study the nonlinear behaviour of microbeams.[11-14] As exact closed-form solutions for complicated nonlinear dynamical systems are often unavailable, various numerical and analytical methods have been proposed for quantitative analysis. Making use of numerical-based approaches, Kuang and Chen[15] examined the dynamic characteristics of fully-fixed micro-actuators via the differential quadrature method. Ghayesh et al.[16] investigated the nonlinear dynamic behavior of electrically actuated MEMS resonators by means of the pseudo-arclength continuation technique. Furthermore, Alsaleem et al.[17] considered the nonlinear resonance and dynamic pull-in instability of MEMS resonators using the finite-difference method. Moghimi Zand[18] applied the Newmark scheme to study the dynamic pull-in instability and snap-through buckling of initially curved MEMS resonators. Using the Runge-Kutta method, Dantas

and Gusso[19] extended to investigate the chaotic dynamics of doubly-clamped beam MEMS resonators.

Although numerical methods can be used to accurately predict the dynamic response of MEMS resonators, they are not able to provide an all-encompassing view for the investigation of nonlinear systems in response to changes in physical parameters. Therefore, various analytical approximation approaches, e.g., multiple scale, harmonic balance and perturbation-based methods, have been used for studying MEMS systems. For instance, Younis and Nayfeh[20] formulated analytical expressions for the dynamic response of resonators. Zhang and Meng[21] conducted the nonlinear dynamic analysis of MEMS sensors under a parametric force excitation. Elshurafa et al.[22] studied the nonlinear dynamics of folded MEMS resonators. Rezazadeh et al.[23] analyzed the parametric oscillation of microbeams. Moreover, Caruntu et al.[24,25] investigated the nonlinear response of micro-resonators under a near-half natural frequency and presented steady-state solutions for MEMS cantilever resonators. Qian et al.[26] derived periodic solutions for a high-order nonlinear oscillator that arises in MEMS systems. Han et al.[27,28] predicted the existence of bifurcation and chaotic motion of fully-clamped MEMS resonators with two symmetrically actuated electrodes. Li and Zhang[29] further made deeper insights on the bi-stable effect of microbeam systems. More recently, Saadatmand and Shooshtari[30] also performed the forced nonlinear vibration analysis of circular micro-plates in two-sided MEMS capacitive systems.

To further refine the accuracy and flexibility of analytical approximation approaches, Wu et al.[31] proposed the Newton harmonic balance (NHB) method that is capable of solving large-amplitude oscillation of strongly nonlinear systems. Subsequently, the NHB has been extended to deal with nonlinear conservative asymmetric oscillators[32,33], strongly damped nonlinear oscillation problems[34] and harmonically forced oscillation systems[35]. In order to achieve a faster convergence rate, an improved version of the NHB method has recently been presented.[36] Because of its simplification and effectiveness, this method has also been applied to investigate the nonlinear dynamics and post-buckling behavior of MEMS systems.[37-39]

The present study focuses on both free and forced nonlinear vibration of doubly-clamped MEMS microbeams. Effects of the mid-plane stretching, axial residual stress and electrostatic force are considered. Specifically, the free vibration of a doubly-clamped microbeam suspended on an electrode due to a suddenly applied DC voltage is considered.[40] Unlike the previous work[39], we further consider the fringing field effect and electrostatic loads in this model. Based on the

Euler-Bernoulli beam theory and the von Karman type nonlinear kinematics, the nonlinear integral-differential governing equation can be further converted to an ordinary differential equation by the Galerkin method and then solved by the NHB method. In addition, the harmonically forced vibration of a doubly-clamped microbeam sandwiched by two symmetric electrodes is also investigated.[27,28] The electrodes are connected by a DC voltage and a harmonic AC voltage. Following the same decomposition principle, the governing equation is also converted to an ordinary differential equation with odd nonlinearity.

This paper is organized as follows. Sections 2 and 3 present the mathematical formulations for both illustrative cases and its solution methodologies, respectively. Section 4 shows the accuracy of the present solutions for both cases in contrast to the results obtained from the Runge-Kutta method. Finally, Section 5 concludes the research findings of this work.

2. Mathematical formulation

Two schematic diagrams for a doubly clamped microbeam model are shown in Fig. 1. In these diagrams, one microbeam is suspended on a rigid electrode, while the other one is sandwiched by two symmetric rigid electrodes. We consider the microbeam of length L, width b and thickness h. The initial gap between the microbeam and the electrode is d. The coordinates *x*, *y* and *z* are along the beam length, width and thickness, respectively. We assume that the actuation voltage is $V(t) = V_{dc} + V_{ac}\cos(2\pi\tilde{f}t)$, where V_{dc} is the bias DC voltage, and V_{ac} and $\tilde{f}$ are the amplitude and frequency of the excited AC voltage, respectively. From a physics perspective, the bias DC voltage and the excited AC voltage are connected in series. This form of excitation can provide a pathway for tuning various effects on MEMS resonators.[1, 3, 5]

Employing the classical beam theory and the von Karman nonlinearity, the transverse deflection of a microbeam with one-sided/two-sided electrodes can be expressed as follows[18,20,40]

$$\rho bh\frac{\partial^2 w}{\partial t^2} + c\frac{\partial w}{\partial t} + EI\frac{\partial^4 w}{\partial x^4} - \left[N_i + \frac{Ebh}{2L}\int_0^L \left(\frac{\partial w}{\partial x}\right)^2 dx\right]\frac{\partial^2 w}{\partial x^2} = F_e \tag{1}$$

where *w* is the deflection in the *z*-direction, *c* is the damping coefficient, *I* is the moment of inertia of the cross section, *E* is the effective Young's modulus of the beam ($= E'/\left(1-\upsilon^2\right)$ with E' = Young's modulus and υ = Poisson ratio), N_i is an initial axial load due to the residual stress on the

beam, F_e is the electrostatic force per unit length, and t is time. When the microbeam is suspended on an electrode, we consider[40]

$$F_e = \frac{1}{2}\frac{b\varepsilon_0 V^2(t)}{(d-w)^2}\left[1+\beta\frac{(d-w)}{b}\right] \tag{2}$$

In another case, when the microbeam is suspended between two symmetric electrodes, the electrostatic force becomes[27]

$$F_e = \frac{1}{2}\varepsilon_0 b\left\{\frac{\left[V_{dc}+V_{ac}\cos(2\pi\tilde{f}t)\right]^2}{(d-w)^2}-\frac{V_{dc}^2}{(d+w)^2}\right\} \tag{3}$$

where ε_0 is the permittivity of the gap medium.

In Eq. (2), β is a parameter that is used to account for the "*fringing field effect*" due to the finite width of the microbeam. For a doubly-clamped beam, β is set to be 0.65.[7,40] The fringing field effect for the microbeam with two-sided electrodes is much smaller than that with one-sided electrode due to the symmetric configuration of the electrodes. Hence, we can ignore the fringing field effect in Eq. (3).

A doubly-clamped microbeam is imposed to the following boundary conditions

$$w(0,t)=0,\quad \frac{\partial w(0,t)}{\partial x}=0 \tag{4a}$$

$$w(L,t)=0,\quad \frac{\partial w(L,t)}{\partial x}=0 \tag{4a}$$

Before the electrostatic actuation, the initial conditions are

$$w(x,0)=0,\quad \frac{\partial w(x,0)}{\partial t}=0 \tag{5}$$

For convenience and brevity, the dimensionless quantities are defined as follows

$$\tau=\sqrt{\frac{EI}{\rho bhL^4}}t,\ W=\frac{w}{d},\ \xi=\frac{x}{L},\ \tilde{c}=\frac{cL^2}{\sqrt{\rho EIbh}},\ f_i=\frac{N_iL^2}{EI},\ \alpha=6\left(\frac{d}{h}\right)^2,$$
$$\lambda^2=\frac{24\varepsilon_0L^4}{Eh^3d^3},\ \gamma=\frac{d}{b},\ f=\sqrt{\frac{\rho bhL^4}{EI}}\tilde{f} \tag{6}$$

in which τ, W, ξ, $\tilde{c}$ and f are the dimensionless time, beam deflection, longitudinal coordinate, damping parameter and AC voltage frequency, respectively. By utilizing Eq. (6), the dimensionless equation of motion for Eq. (1) is given by

$$\frac{\partial^2 W}{\partial \tau^2}+\tilde{c}\frac{\partial W}{\partial \tau}+\frac{\partial^4 W}{\partial \xi^4}-\left[f_i+\alpha\int_0^1\left(\frac{\partial W}{\partial \xi}\right)^2 d\xi\right]\frac{\partial^2 W}{\partial \xi^2}=F_{es} \tag{7}$$

where

$$F_{es}=\frac{\lambda^2 V^2(t)}{4(1-W)^2}[1+\gamma\beta(1-W)] \tag{8}$$

for the microbeam with one-sided electrode, and

$$F_{es}=\lambda^2 {V_{dc}}^2\frac{W}{(1-W^2)^2}+\frac{1}{4}\lambda^2\left[\frac{2V_{dc}V_{ac}\cos(2\pi f\tau)+{V_{ac}}^2\cos^2(2\pi f\tau)}{(1-W)^2}\right] \tag{9}$$

for the microbeam with two-sided electrodes.

The corresponding dimensionless boundary conditions become

$$W(0,\tau)=0,\quad \frac{\partial W(0,\tau)}{\partial \xi}=0 \tag{10a}$$

$$W(1,\tau)=0,\quad \frac{\partial W(1,\tau)}{\partial \xi}=0 \tag{10b}$$

and the dimensionless initial conditions are

$$W(\xi,0)=0,\quad \frac{\partial W(\xi,0)}{\partial \tau}=0 \tag{11}$$

As we only concentrate on investigating the first-mode natural frequency and the primary resonance of the microbeam in this work, the deflection function of the microbeam can be approximated as a product of two functions with a sustainable error in accordance with the Galerkin method. The deflection function is expressed as

$$W(\xi,\tau)=\phi(\xi)q(\tau) \tag{12}$$

where $\phi(\xi)$ is the assumed deflection shape function that corresponds to the first mode shape and satisfies the boundary conditions given in Eq. (10), and $q(\tau)$ is the mid-point deflection of the microbeam. A reasonable deflection shape function for the first mode shape of Eq. (7) is[40]

$$\phi(\xi)=\left[\cosh(\lambda_1\xi)-\cos(\lambda_1\xi)\right]-\frac{\cosh(\lambda_1)-\cos(\lambda_1)}{\sinh(\lambda_1)-\sin(\lambda_1)}\left[\sinh(\lambda_1\xi)-\sin(\lambda_1\xi)\right] \tag{13}$$

in which $\lambda_1 = 4.730040745$.

2.1 Case 1: Asymmetric vibration of a doubly-clamped microbeam with one-sided electrode due to a suddenly applied DC voltage

Consider the MEMS device in Fig. 1a, the electrostatic actuation (i.e., DC voltage) first makes the microbeam deflect to an equilibrium configuration, and then it vibrates asymmetrically around the equilibrium position due to an AC voltage. For free and undamped vibration, we first compute the natural frequencies of the microbeam, the AC voltage and the damping term in Eqs. (7) and (8) should be set to zero. Substituting Eq. (12) into Eq. (7) and applying the Galerkin procedure, the governing partial differential equation can be converted to a nonlinear ordinary differential equation as follows

$$\frac{d^2q}{d\tau^2}+\alpha_1 q+\alpha_2 q^3-\frac{\lambda^2 {V_{dc}}^2}{4}\int_0^1 \frac{\phi}{(1-q\phi)^2}\left[1+\gamma\beta(1-q\phi)\right]d\xi=0 \tag{14}$$

with the following initial conditions

$$q(0)=0,\quad \frac{dq(0)}{d\tau}=0 \tag{15}$$

where $\alpha_1=\int_0^1\left(\frac{d^4\phi}{d\xi^4}-f_i\frac{d^2\phi}{d\xi^2}\right)\phi d\xi$ and $\alpha_2=-\alpha\int_0^1\left(\frac{d\phi}{d\xi}\right)^2 d\xi\int_0^1\left(\frac{d^2\phi}{d\xi^2}\right)\phi d\xi$.

It is noted that analytical approximation solutions for the free vibration of the nonlinear system (14) cannot be directly obtained by the NHB method, as the electrostatic force term is not able to be integrated analytically. To deal with this scenario, instead of approximating it using a Taylor series expansion around the initial configuration $q = 0$, it is performed to expand this term around the equilibrium position. This is because the free vibration of the microbeam occurs around its equilibrium position (i.e., $q = q_0$) rather than its initial position (i.e., $q = 0$). The accuracy of the two approximation methods can be verified below.

Incorporating a Taylor series expansion,[39] we expand the integral part in Eq. (14) up to fourth-order terms around the initial position and the equilibrium position of the microbeam in Eqs. (16) and (17), respectively, we have

$$\frac{d^2q}{d\tau^2}+\alpha_1 q+\alpha_2 q^3+\sum_{n=0}^{4}L_n q^n=0 \tag{16}$$

$$\frac{d^2q}{d\tau^2}+\alpha_1 q+\alpha_2 q^3+\sum_{n=0}^{4}K_n (q-q_0)^n=0 \tag{17}$$

where $L_n=-\frac{\lambda^2 {V_{dc}}^2}{4}\int_0^1(n+1+\gamma\beta)\varphi^{n+1}d\xi$ and $K_n=-\frac{\lambda^2 {V_{dc}}^2}{4}\int_0^1\frac{[n+1+\gamma\beta(1-q_0\varphi)]\varphi^{n+1}}{(1-q_0\varphi)^{n+2}}d\xi$.

The exact value of the equilibrium position can be calculated iteratively according to the principle that the restoring force of the microbeam at the equilibrium position in Eq. (14) is zero, i.e.,

$$\alpha_1 q_0 + \alpha_2 q_0^3 - \frac{\lambda^2 V_{dc}^{\ 2}}{4}\int_0^1 \frac{\phi}{(1-q_0\phi)^2}\left[1+\gamma\beta(1-q_0\phi)\right]d\xi = 0 \tag{18}$$

As a case study, numerical calculations are performed for the dynamic analysis of a microbeam with the geometrical and material parameters given in Table 1. Fig. 2 shows the values of the equilibrium position of the microbeam under various electrostatic actuations V_{dc}.

For comparison, we refer the systems (14), (16) and (17) as models 1, 2 and 3, respectively. Indeed, the use of a Taylor series expansion around the initial position q = 0 has been used for analysis by using the homotopy analysis method.[40] By only changing the length of the microbeam, values of the dynamic pull-in voltage of the microbeam for the three models are calculated in accordance with the principle of energy conservation. Note that the dynamic pull-in instability occurs when there is no solution to the deflection q in the range of (0, 1) where has the same energy level with the initial conditions. In Table 2, it is obvious that the results of model 3 are much closer to that of model 1 than that of model 2. Among various cases in Table 2, the maximum relative error of the dynamic pull-in voltage values between model 1 and model 3 is only 0.7% for L = 210 μm, but it is up to 4.3% between model 1 and model 2. Besides, the results for the restoring force of the three models under an input voltage (25 V) are depicted in Fig. 3. The circle dots represent the exact solution, while the dashed line and solid line correspond to the two approximation models, respectively, i.e., Eqs. (16) and (17). It is observed that the results of the three models have an excellent agreement with each other when the deflection is small. For q > 0.2, there is a significant discrepancy. Specifically, the solid line is much closer to the circle dots than the dashed line, it refers that the integral term in Eq. (14) approximated by a Taylor series at the equilibrium position has a greater accuracy than that at the initial position. Hence, the system (17) is used for the subsequent analysis.

For convenience and brevity, a new variable is introduced as follows

$$u = q - q_0 \tag{19}$$

Then, Eq. (17) can be rewritten as

$$u'' + g(u) = 0 \tag{20}$$

with

$$u(0) = -q_0, \quad u'(0) = 0 \tag{21}$$

where a prime donates differentiation with respect to τ. The restoring force function of Eq. (20) is $g(u) = \beta_1 u + \beta_2 u^2 + \beta_3 u^3 + \beta_4 u^4$, in which $\beta_1 = \alpha_1 + 3\alpha_2 q_0^2 + K_1$, $\beta_2 = 3\alpha_2 q_0 + K_2$, $\beta_3 = \alpha_2 + K_3$ and $\beta_4 = K_4$. In this system, the potential energy is given by

$$P(u) = \frac{1}{2}\beta_1 u^2 + \frac{1}{3}\beta_2 u^3 + \frac{1}{4}\beta_3 u^4 + \frac{1}{5}\beta_4 u^5 \tag{22}$$

and the system (20) can be solved analytically in accordance with Sections 3.1 and 3.2.

2.2 Case 2: Resonance response of a doubly-clamped microbeam with two-sided electrodes actuated by a bias DC voltage and a AC harmonic voltage

Consider the MEMS model in Fig. 1(b), the initial position is a stable equilibrium position for the microbeam. In this case, the DC voltage is acted as a bias one and the microbeam is driven by the AC voltage to vibrate symmetrically around its initial position. Here, we focus on the investigation of resonance responses when the actuating frequency is close to the first natural frequency of the microbeam. For a small AC voltage ($V_{ac} << V_{dc}$), we neglect the terms with V_{ac}^2, Eq. (7) can be further simplified as

$$\frac{\partial^2 W}{\partial \tau^2} + \tilde{c}\frac{\partial W}{\partial \tau} + \frac{\partial^4 W}{\partial \xi^4} - \left[f_i + \alpha \int_0^1 \left(\frac{\partial W}{\partial \xi} \right)^2 d\xi \right] \frac{\partial^2 W}{\partial \xi^2} - \lambda^2 V_{dc}^2 W \left(1 + 2W^2 + 3W^4 \right) = \frac{1}{2}\lambda^2 V_{dc} V_{ac} \cos\left(2\pi f \tau \right) \tag{23}$$

By means of a Taylor series expansion, the electrostatic force term is generally expanded up to the fifth-order term near the initial position $q = 0$ and the higher-order terms are ignored.

Substituting Eq. (12) into Eq. (23) and applying the Galerkin procedure, the nonlinear governing equation of motion can be written as

$$\frac{d^2 q}{d\tau^2} + \tilde{c}\frac{dq}{d\tau} + (\beta_1 + \alpha_1) q + (\beta_2 + \alpha_2) q^3 + \alpha_3 q^5 = F_0 \cos(2\pi f \tau) \tag{24}$$

where $F_0 = \frac{1}{2}\lambda^2 V_{dc} V_{ac} \int_0^1 \phi d\phi$, $\beta_1 = \int_0^1 \left(\frac{d^4\phi}{d\xi^4} - f_i \frac{d^2\phi}{d\xi^2} \right) \phi d\phi$, $\beta_2 = \int_0^1 \left(-\alpha \frac{d^2\phi}{d\xi^2} \int_0^1 \left(\frac{d\phi}{d\xi} \right)^2 d\xi \right) \phi d\phi$, and $\alpha_i = -i\lambda^2 V_{dc}{}^2 \int_0^1 \phi^{2i} d\phi (i = 1, 2, 3)$.

For further simplication, Eq. (24) can be expressed as

$$\omega^2 \frac{d^2 q}{d\tilde{\tau}^2} + f(q) + g\left(\omega \frac{dq}{d\tilde{\tau}}\right) = F_0 \cos\tilde{\tau} \tag{25}$$

where $f(q) = (\beta_1 + \alpha_1)q + (\beta_2 + \alpha_3)q^3 + \alpha_5 q^5$, $g(p) = \tilde{c}p$ $(p = dq/d\tau)$ and $\tilde{\tau} = \omega\tau$. The first-order and second-order analytical approximations to the frequency-amplitude response for the system (25) can be obtained in accordance with Section 3.3 below.

3. Solution approaches

This section briefly introduces the NHB method to solve the free and forced vibration of nonlinear systems.

3.1 Analytical approximation solutions for strongly odd nonlinear conservative system

Following the NHB method and its improved version,[31,36] we consider a nonlinear system governed by

$$\frac{d^2 x}{dt^2} + g(x) = 0, \quad g(x) = -g(-x) \tag{26}$$

with the initial conditions

$$x(0) = -A \ (A > 0), \quad \frac{dx(0)}{dt} = 0 \tag{27}$$

The first-order $x_1(t)$, second-order $x_2(t)$ and improved second-order $x_2^*(t)$ analytical approximations are given by

$$x_1(t) = A\cos\left[\omega_1\left(t - \frac{T}{2}\right)\right], \quad \omega_1 = \sqrt{\Omega_1} \tag{28}$$

$$x_2(t) = (A + y_1)\cos\left[\omega_2\left(t - \frac{T}{2}\right)\right] - y_1\cos\left[3\omega_2\left(t - \frac{T}{2}\right)\right], \quad \omega_2 = \sqrt{\Omega_2} \tag{29}$$

$$x_2^*(t) = (A + y_2)\cos\left[\omega_2^*\left(t - \frac{T}{2}\right)\right] + (-y_2 + y_3)\cos\left[3\omega_2^*\left(t - \frac{T}{2}\right)\right] - y_3\cos\left[5\omega_2^*\left(t - \frac{T}{2}\right)\right], \tag{30}$$

$$\omega_2^* = \sqrt{\Omega_2^*}$$

where

$$\Omega_1 = -\frac{a_1}{A},$$

$$\Omega_2 = \Omega_1 + \Delta\Omega_1,$$

$$\Omega_2^* = \Omega_1 + \Delta\Omega_1^*,$$

$$\Delta\Omega_1 = -\frac{a_3\left[\left(b_0 - b_4\right)A - 2a_1\right]}{A\left[\left(b_2 + b_4 - b_0 - b_6\right)A + 18a_1\right]},$$

$$\Delta\Omega_1^* = \frac{a_3\left(M_3N_1 - M_1N_3\right) + a_5\left(M_1N_2 - M_2N_1\right)}{A\left(M_2N_3 - M_3N_2\right)},$$

$$y_1 = -\frac{2a_3A}{(b_2 + b_4 - b_0 - b_6)A + 18a_1},$$

$$y_2 = \frac{-N_3a_3 + N_2a_5}{M_2N_3 - M_3N_2},$$

$$y_3 = \frac{M_3a_3 - M_2a_5}{M_2N_3 - M_3N_2},$$

$$M_1 = \frac{1}{8}\left[\frac{-8a_1}{A} - 8\Delta\Omega_1 + 4b_0 - 4b_4 + y_1(3c_1 - 3c_3 - c_5 + c_7)\right],$$

$$N_1 = \frac{1}{8}\left[4b_2 - 4b_6 + y_1(2c_3 - 2c_5 - c_7 + c_9)\right],$$

$$M_2 = \frac{1}{8}\left[\frac{72a_1}{A} + 72\Delta\Omega_1 - 4b_0 + 4b_2 + 4b_4 - 4b_6 + y_1(-3c_1 + 5c_3 - c_5 - 2c_7 + c_9)\right],$$

$$N_2 = \frac{1}{8}\left[\frac{-72a_1}{A} - 72\Delta\Omega_1 + 4b_0 - 4b_2 + 4b_6 - 4b_8 + y_1(2c_1 - 4c_3 + 3c_5 - 2c_9 + c_{11})\right],$$

$$M_3 = \frac{1}{8}\left[-4b_2 + 4b_4 + 4b_6 - 4b_8 - y_1(c_1 + c_3 - 4c_5 + c_7 + 2c_9 - c_{11})\right] \text{ and}$$

$$N_3 = \frac{1}{8}\left[\frac{200a_1}{A} + 200\Delta\Omega_1 - 4b_0 + 4b_2 + 4b_8 - 4b_{10} + y_1(-2c_1 + 3c_3 - 2c_5 + 2c_7 - 2c_{11} + c_{13})\right].$$

237 Here, a_i, b_i and c_i are the Fourier series coefficients that can be determined by

$$a_{2i-1} = \frac{4}{\pi}\int_0^{\pi/2} g(x)\cos[(2i-1)\tau]d\tau, \qquad i = 1, 2, 3, \cdots,$$

$$b_{2(i-1)} = \frac{4}{\pi}\int_0^{\pi/2} g_x(x)\cos[2(i-1)\tau]d\tau, \qquad i = 1, 2, 3, \cdots \text{ and}$$

$$c_{2i-1}=\frac{4}{\pi}\int_0^{\pi/2} g_{xx}(x)\cos[(2i-1)\tau]d\tau,\qquad i=1,2,3,\cdots.$$

The subscript x denotes the derivative of $g(x)$ with respect to x.

3.2 Analytical approximation solutions for strongly general nonlinear conservative system

Consider the following nonlinear system governed by a general restoring force

$$\frac{d^2x}{dt^2}+g\left(x\right)=0,\quad g\left(x\right)\neq -g\left(-x\right) \tag{31}$$

with the initial conditions

$$x\left(0\right)=-A\left(A>0\right),\quad \frac{dx}{dt}\left(0\right)=0 \tag{32}$$

The system oscillates between an asymmetric bound $\left[-A,B\right]$ where $B\left(B>0\right)$ and $-A$ have the same energy level, i.e.,

$$P(B)=P(-A) \tag{33}$$

where $P(x)=\int g(x)dx$ is the potential energy of the system.

To deal with such a case, two newly nonlinear systems with odd nonlinearity are introduced in Eqs. (34) and (35).[41] Both of them can be solved separately by the NHB method as described in Section 3.1.

$$\frac{d^2x}{dt^2}+J\left(x\right)=0,\quad x\left(0\right)=-A,\ \frac{dx}{dt}\left(0\right)=0 \tag{34}$$

and

$$\frac{d^2x}{dt^2}+K\left(x\right)=0,\quad x\left(0\right)=-B,\ \frac{dx}{dt}\left(0\right)=0 \tag{35}$$

where

$$J\left(x\right)=\begin{cases} g\left(x\right), & x\geq 0\\ -g\left(-x\right), & x<0\end{cases}$$

and

$$K\left(x\right)=\begin{cases} -g\left(-x\right), & x>0\\ g\left(x\right), & x\leq 0\end{cases}$$

Then, the analytical approximation solutions for the asymmetric oscillation of the system (31) can be constructed and presented in Eqs. (36)-(41).

The first-order analytical frequency ω_1 and periodic solution $x_1(t)$ of the system (31) are

$$\omega_1 = \frac{2\omega_{11}\omega_{12}}{\omega_{11}+\omega_{12}} \tag{36}$$

$$x_1(t) = \begin{cases} x_{11}(t), & 0 \le t \le \dfrac{T_{11}}{4} \\ x_{12}\left(t - \dfrac{T_{11}}{4} + \dfrac{T_{12}}{4}\right), & \dfrac{T_{11}}{4} < t \le \dfrac{T_{11}}{4} + \dfrac{T_{12}}{2} \\ x_{11}\left(t + \dfrac{T_{11}}{2} - \dfrac{T_{12}}{2}\right), & \dfrac{T_{11}}{4} + \dfrac{T_{12}}{2} < t \le \dfrac{T_{11}}{2} + \dfrac{T_{12}}{2} \end{cases} \tag{37}$$

where the subscripts "11" and "12" of ω, T and $x(t)$ denote the corresponding first-order analytical solutions for the systems (34) and (35), respectively.

The second-order analytical frequency ω_2 and solution $x_2(t)$ of the system (31) are

$$\omega_2 = \frac{2\omega_{21}\omega_{22}}{\omega_{21}+\omega_{22}} \tag{38}$$

$$x_2(t) = \begin{cases} x_{21}(t), & 0 \le t \le \dfrac{T_{21}}{4} \\ x_{22}\left(t - \dfrac{T_{21}}{4} + \dfrac{T_{22}}{4}\right), & \dfrac{T_{21}}{4} < t \le \dfrac{T_{21}}{4} + \dfrac{T_{22}}{2} \\ x_{21}\left(t + \dfrac{T_{21}}{2} - \dfrac{T_{22}}{2}\right), & \dfrac{T_{21}}{4} + \dfrac{T_{22}}{2} < t \le \dfrac{T_{21}}{2} + \dfrac{T_{22}}{2} \end{cases} \tag{39}$$

where the subscripts "21" and "22" of ω, T and $x(t)$ denote the corresponding second-order analytical solutions for the systems (34) and (35), respectively.

The improved second-order analytical frequency ω_2^* and periodic solution $x_2^*(t)$ of the system (31) are

$$\omega_2^* = \frac{2\omega_{21}^*\omega_{22}^*}{\omega_{21}^*+\omega_{22}^*} \tag{40}$$

$$x_2^*(t)=\begin{cases} x_{21}^*(t), \quad 0\le t\le \dfrac{T_{21}^*}{4} \\ x_{22}^*\left(t-\dfrac{T_{21}^*}{4}+\dfrac{T_{22}^*}{4}\right), \quad \dfrac{T_{21}^*}{4}<t\le \dfrac{T_{21}^*}{4}+\dfrac{T_{22}^*}{2} \\ x_{21}^*\left(t+\dfrac{T_{21}^*}{2}-\dfrac{T_{22}^*}{2}\right), \quad \dfrac{T_{21}^*}{4}+\dfrac{T_{22}^*}{2}<t\le \dfrac{T_{21}^*}{2}+\dfrac{T_{22}^*}{2} \end{cases} \tag{41}$$

where the subscripts "21" and "22" of ω^*, T^* and $x^*(t)$ denote the corresponding improved second-order analytical solutions for the systems (34) and (35), respectively.

3.3 Analytical approximation solutions for harmonically forced odd nonlinear system

Building upon the framework of the NHB approach,[31] we further consider the steady-state response of a harmonically forced odd nonlinear system near its first frequency.[35] The equation of motion is given by

$$\frac{d^2u}{dt^2}+f(u)+g\left(\frac{du}{dt}\right)=F_0\cos(\omega t) \tag{42}$$

where $f(u)$ and $g(v)(v=du/dt)$ are odd functions of u and v, respectively. Firstly, a new independent variable $\tilde{\tau}=\omega t$ is introduced and Eq. (42) is transformed to

$$\omega^2\frac{d^2u}{d\tilde{\tau}^2}+f(u)+g\left(\omega\frac{du}{d\tilde{\tau}}\right)=F_0\cos(\tilde{\tau}+\theta) \tag{43}$$

where θ represents the phase difference between the external excitation and the steady-state response. It has been added in the excitation so that we can construct a response with phase zero. For the steady-state response of Eq. (42), the following boundary conditions are imposed

$$u(0)=u(2\pi)=A,\ \ u'(0)=u'(2\pi)=0 \tag{44}$$

where A is the amplitude of a steady-state response.

The periodic solution $u(\tau)$ to Eq. (42) is represented by a Fourier series that contains odd multiples of $\tilde{\tau}$ only

$$u(\tilde{\tau})=M_1\cos\tilde{\tau}+\sum_{n=1}^{\infty}M_{2n+1}\cos(2n+1)\tilde{\tau}+\sum_{n=1}^{\infty}N_{2n+1}\sin(2n+1)\tilde{\tau} \tag{45}$$

277 Making use of a single-term HB method, the first-order analytical approximation to $u(\tilde{\tau})$, A, ω
278 and θ are assumed as

$$u_1(\tilde{\tau}) = A\cos\tilde{\tau},\ A = A_1,\ \ \omega = \omega_1,\ \ \theta = \theta_1 \tag{46}$$

279 Substituting Eq. (46) into Eq. (42), expanding the resulting expression into a trigonometric series
280 and setting the coefficients of $\sin\tilde{\tau}$ and $\cos\tilde{\tau}$ to zero, we have

$$\left(-\omega_1^2 A_1 + a_1\right)^2 + c_1^2 = F_0^2 \tag{47}$$

281 and

$$\tan\theta_1 = \frac{c_1}{\omega_1^2 A_1 - a_1} \tag{48}$$

282 where $a_1 = \frac{4}{\pi}\int_0^{\pi/2} f(A_1\cos\tilde{\tau})\cos\tilde{\tau}\,d\tilde{\tau}$ and $c_1 = \frac{4}{\pi}\int_0^{\pi/2} g(-\omega A_1\sin\tilde{\tau})\sin\tilde{\tau}\,d\tilde{\tau}$.

283 Subsequently, the second-order analytical approximations to $u(\tilde{\tau})$, A, ω and θ are
284 expressed by adding increments to the first-order analytical approximation as follows

$$u_2 = u_1 + \Delta u_1,\ \ A_2 = A_1 + \Delta A_1,\ \ \omega_2 = \omega_1 + \Delta\omega_1,\ \ \theta_2 = \theta_1 + \Delta\theta_1 \tag{49}$$

285 where $\Delta u_1 = \Delta A_1\cos\tilde{\tau} + C_1\left(\cos\tilde{\tau} - \cos 3\tilde{\tau}\right) + S_1\left(\frac{\sin 3\tilde{\tau}}{3} - \frac{\sin 5\tilde{\tau}}{5}\right)$.

286 Substituting Eq. (49) into Eq. (42), linearizing with respect to the increments, expanding the
287 resulting expression in a trigonometric series and setting the coefficients of $\sin\tilde{\tau}$, $\cos\tilde{\tau}$, $\sin 3\tilde{\tau}$
288 and $\cos 3\tilde{\tau}$, we get

$$\mathbf{K}_1 \cdot \mathbf{z}_1 = \mathbf{e}_1 \cdot \Delta\theta_1 + \mathbf{f}_1 \tag{50}$$

289 where

$$\mathbf{K}_1 = \begin{pmatrix} K_{11} & K_{12} & K_{13} & K_{14} \\ K_{21} & K_{22} & K_{23} & K_{24} \\ K_{31} & K_{32} & K_{33} & K_{34} \\ K_{41} & K_{42} & K_{43} & K_{44} \end{pmatrix},$$

$$\mathbf{z}_1 = \left(\Delta\omega_1,\ \ \Delta A_1,\ \ C_1,\ \ S_1\right)^T,$$

$$\mathbf{e}_1 = \left(-F_0\sin\theta_1,\ \ -F_0\cos\theta_1,\ \ 0,\ \ 0\right)^T \text{ and}$$

$$\mathbf{f}_1 = \left(0,\ \ 0,\ \ -a_3,\ \ -c_3\right)^T.$$

290 Here,

$$K_{11}=-2A_1\omega_1,\ K_{12}=\left(-2\omega_1^2+b_0+b_2\right)/2,\ K_{13}=\left(-2\omega_1^2+b_0-b_4\right)/2,$$
$$K_{14}=\omega_1\left(d_2-d_6\right)/2,\ K_{21}=A_1\left(-d_0+d_2\right)/2,\ K_{22}=\omega_1\left(-d_0+d_2\right)/2,$$
$$K_{23}=\omega_1\left(-d_0+4d_2+3d_4\right)/2,\ K_{24}=\omega_1\left(5b_2-8b_4+3b_6\right)/30,$$
$$K_{31}=0,\ K_{32}=\left(b_2+b_4\right)/2,\ K_{33}=\left(18\omega_1^2-b_0+b_2+b_4-b_6\right)/2,$$
$$K_{34}=\omega_1\left(d_0-d_2+d_6-d_8\right)/2,\ K_{41}=A_1\left(-d_2+d_4\right)/2,\ K_{42}=\omega_1\left(-d_2+d_4\right)/2,$$
$$K_{43}=\omega_1\left(3d_0-d_2+d_4-3d_6\right)/2,\ K_{44}=\left(-90\omega_1^2+5b_0-3b_2-5b_6+3b_8\right)/30,$$
$$a_{2n-1}=\frac{1}{\pi}\int_0^{2\pi} f(A_1\cos\tilde{\tau})\cos(2n-1)\tilde{\tau}d\tilde{\tau},(n=1,2,\cdots),$$
$$b_{2n}=\frac{1}{\pi}\int_0^{2\pi} f_u(A_1\cos\tilde{\tau})\cos(2n\tilde{\tau})d\tilde{\tau},(n=0,1,\cdots),$$
$$c_{2n-1}=\frac{1}{\pi}\int_0^{2\pi} g(-\omega A_1\sin\tilde{\tau})\sin(2n-1)\tilde{\tau}d\tilde{\tau},(n=1,2,\cdots)\ \text{and}$$
$$d_{2n}=\frac{1}{\pi}\int_0^{2\pi} g_v(-\omega A_1\sin\tilde{\tau})\cos(2n\tilde{\tau})d\tilde{\tau},(n=0,1,\cdots).$$

With a least-squares sense, the second-order analytical approximation can be derived. Detailed derivations can be referred Ref. [35].

4. Results and Discussion

4.1 Case 1: Asymmetric vibration of a doubly-clamped microbeam with one-sided electrode due to a suddenly applied DC voltage

In this section, approximate solutions obtained through the NHB method for the case in Section 2.1 are presented and compared with those results from the Runge-Kutta method. The geometrical and material parameters of the microbeam can be referred to Table 1. For reference, the exact frequency of the system (17) is given by

$$\omega_e=\frac{2\omega_{e1}\omega_{e2}}{\omega_{e1}+\omega_{e2}} \tag{51}$$

where

$$\omega_{e1}=\pi/\int_0^{\frac{\pi}{2}}\frac{\sqrt{2}A\sin\theta}{\sqrt{P(A)-P(A\cos\theta)}}d\theta\ \text{ and }\ \omega_{e2}=\pi/\int_0^{\frac{\pi}{2}}\frac{\sqrt{2}B\sin\theta}{\sqrt{P(B)-P(B\cos\theta)}}d\theta.$$

The equilibrium points as well as the initial frequencies obtained by the NHB method and the exact frequencies under different input voltages are listed in Table 3. It is observed that the vibration amplitude increases with an increase of the input voltage, while the frequency declines. When the input voltage is low, the first-order, second-order and improved second-order

frequencies all agree well with the exact solution. In addition, when the input voltage is close to the DC dynamic pull-in voltage, the higher-order initial frequencies are still in good agreement with the exact one.

To further illustrate and verify the accuracy for the NHB method, the time-history responses of the microbeam mid-point deflection for the first-order, second-order and improved second-order approximations and the Runge-Kutta results are presented in Figs. 4 and 5. When the value of V_{dc} is close to the DC dynamic pull-in voltage, the improved second-order approximation is still in good agreement with the Runge-Kutta results. However, the first-order approximation is not sufficiently good, see Fig. 5(b).

4.2 Case 2: Resonance response of a doubly-clamped microbeam with two-sided electrodes actuated by a DC voltage and a harmonic AC voltage

In this section, the case study of a doubly-clamped microbeam with two-sided electrodes actuated by a DC voltage and a harmonic AC ovltage is presented. The geometrical and material parameters of the microbeam are given in Table 1. The frequency-amplitude curves derived by the NHB and Runge-Kutta methods for three different sets of electric loads, i.e., (i) V_{dc} = 8 V and V_{ac} = 0.2 V; (ii) V_{dc} = 12 V and V_{ac} = 0.07 V; and (iii) V_{dc} = 16 V and V_{ac} = 0.01 V, are constructed to demonstrate the accuracy of the proposed analytical method and invetigate the steady-state dynamic behavior of the microbeam. The above three examples yield three corresponding sets of the normalized parameters as follows:

(i) $\tilde{c} = 0.123511$, $\beta_1 = 728.474$, $\beta_2 = 561.989$, $\alpha_1 = -136.442$, $\alpha_2 = -505.355$, $\alpha_3 = -1581.48$, $F_0 = 1.41706$;

(ii) $\tilde{c} = 0.104213$, $\beta_1 = 728.474$, $\beta_2 = 561.989$, $\alpha_1 = -306.996$, $\alpha_2 = -1137.05$, $\alpha_3 = -3558.33$, $F_0 = 0.743957$; and

(iii) $\tilde{c} = 0.0686132$, $\beta_1 = 728.474$, $\beta_2 = 561.989$, $\alpha_1 = -545.77$, $\alpha_2 = -2021.42$, $\alpha_3 = -6325.92$, $F_0 = 0.141706$.

Consider the three cases, a comparison of the first-order and second-order approximate frequency-amplitude responses $q_1(\omega)$ and $q_2(\omega)$ and the numerical results $q_{num}(\omega)$ given by the Runge-Kutta method is presented in Figs. 6-8, respectively. Here, the stable and unstable solutions,

335 determined by the Floquet theory,[42] are represented by the solid and dashed lines, respectively.
336 The red and blue lines, respectively, denote to the first-order and second-order analytical
337 approximations of the frequency-amplitude responses, while the black circle dots represent the the
338 Runge-Kutta results. In Figs 6-8, the analytical approximation and numerical solutions are mainly
339 consistent in the whole fruquency range, even at the resonant fequency. In order to get a closer
340 investigation, Figs. 6(c), 7(c) and 8(c) respectively depict the corresponding absolute errors
341 between $q_1(\omega)$, $q_2(\omega)$ and $q_{num}(\omega)$ in each case between two jumping points. These figures
342 clearly indicate that the second-order analytical approximation provides better solutions to the
343 numerical results.

344 The primary rasonant response of the nonlinear system is examined by varying the excitation
345 frequency around the first linear natural frequency of the system. It is noted that the first natural
346 frequency of the microbeam decreases with increasing the DC voltage. As we observe from these
347 figures, the first non-dimensional natural frequencies of the microbeam for the three cases are
348 24.33, 20.53 and 13.52, respectively.

349 In this model, we consider the effects of electrostatic force and geometrical nonlinearity on
350 the system. The nonlinear electrostatic force tends to yield a softening behavior while the
351 geometrical nonlinearity tends to yield a hardening behavior. It is observed that nonlinearity caused
352 by the electrostatic force is dominant in these three cases since the nonlinear resonance peaks are
353 all bent to the left-hand side. Besides, the amplitude at the mid-point of the microbeam increases
354 as the excitation frequency decreases from a value that is larger than the coresponding first linear
355 frequency until reaching to point A, i.e., nonlinear resonance. At this point, the motion becomes
356 unstable via a limited point bifurcation, thereby causing the system to jump to the lower-amplitude
357 stable branch, as indicated by the black arrows. The system shows different dynamic responses as
358 the excitation frequency increases from a low value. In this case, the instability occurs at point B
359 due to a limited point bifurcation. The system then jumps to the upper-amplitude stable branch as
360 indicated by the black arrows.
361

362 **5. Conclusions**

363 The nonlinear free and forced vibration responses of MEMS microbeams are studied in this
364 work. We mainly focus on the development of lower-order analytical approximation solutions

based on the NHB method for such problems, in which simple and accurate analytical expressions can be obtained. On one hand, the asymmetric vibration of a doubly-clamped microbeam with one-sided electrode due to a suddenly applied DC voltage is investigated. The integral-differential governing equation of this beam model is transformed to a second-order ordinary differential equation having odd and even nonlinearities through the Galerkin method. As the electrostatic force term of this nonlinear system is not able to be integrated analytically, such that it is expanded using a Taylor series around the equilibrium position of this system. The resultant nonlinear equation can then be solved by the NHB method. The analytical approximation solutions are in excellent agreement with those results obtained by the Runge-Kutta method for the whole dynamic range. By increasing the input voltage, the vibration amplitude increases but the frequency declines. On the other hand, the primary resonance effect of a doubly-clamped microbeam with two-sided symmetric electrostatic actuations as well as a harmonically electrostatic load on one side is also studied. Accurate frequency-amplitude responses of the microbeam are derived by means of the analytical approach. By comparing different sets of electrostatic loads, the relationship between the vibration amplitude and natural frequncy of the microbeam is established. It is found that a softening behavior due to the nonlinear electrostatic force is a dominant effect in this case. Based on the present approach, this offers an efficient and reliable avenue to further investigate the nonlinear dynamics of complex MEMS systems subjected to various external excitations.

Acknowledgements

The work described in this paper was fully supported by the National Natural Science Foundation of China (Grant No. 11602210) and the Matching Grant from the Hong Kong Polytechnic University (Project No. 4-BCDS).

References

1. M.I. Younis and F.M. Alsaleem, Exploration of new concepts for mass detection in electrostatically-actuated structures based on nonlinear phenomena. Journal of Computational and Nonlinear Dynamics, vol. 4, 021010, 2009.
2. J.H. Zhao, S.J. Yu, K. Li, Y. Dong, Q. Zhou, and Z. You, Improvement of a micro-beam in a smart gas sensor with resonating mechanism. Proceedings of the 4th IEEE International Conference on Nano/Micro Engineered and Molecular Systems, pp. 371-375, 2009.
3. J.F. Rhoads, S.W. Shaw, and K.L. Turner, Nonlinear dynamics and its applications in micro- and nanoresonators. Journal of Dynamic Systems, Measurement and Control, vol. 132, 034001, 2010.
4. S. Zaitsev, O. Shtempluck, E. Buks, and O. Gottlieb, Nonlinear damping in a micromechanical oscillator. Nonlinear Dynamics, vol. 67, pp. 859-883, 2012.
5. E.M. Abdel-Rahman, M.I. Younis, and A.H. Nayfeh, Characterization of the mechanical behavior of an electrically actuated microbeam. Journal of Micromechanics and Microengineering, vol. 12, pp. 759-766, 2002.
6. R.C. Batra, M. Porfiri, and D. Spinello, Vibrations of narrow microbeams predeformed by an electric field, Journal of Sound and Vibration, vol. 309, pp. 600-612, 2008.
7. X.L. Jia, J. Yang, S. Kitipornchai, and C.W. Lim, Free vibration of geometrically nonlinear micro-switches under electrostatic and Casimir forces, Smart Materials and Structures, vol. 19, 115028, 2010.
8. W.M. Zhang, H. Yan, Z.K. Peng, and G. Meng, Electrostatic pull-in instability in MEMS/NEMS: A review, Sensors and Actuators A: Physical, vol. 214, pp. 187-218, 2014.
9. J.D. Zook, D.W. Burns, H. Guckel, J.J. Sniegowski, R.L. Engelstad, and Z. Feng, Characteristics of polysilicon resonant microbeams. Sensors and Actuators A: Physical, vol. 35, pp. 51-59, 1992.
10. F. Ayela and T. Fournier, An experimental study of anharmonic micromachined silicon resonators. Measurement Science and Technology, vol. 9, pp. 1821-1830, 1998.
11. H.A.C. Tilmans and Legtenberg, R., Electrostatically driven vacuum-encapsulated polysilicon resonators: Part II. Theory and performance. Sensors and Actuators A: Physical, vol. 45, pp. 67-84, 1994.

12. R.M.C. Mestrom, R.H.B. Fey, J.T.M. Van Beek, K.L. Phan and H. Nijmeijer, Modelling the dynamics of a MEMS resonator: simulations and experiments. Sensors and Actuators A: Physical, vol. 142, pp. 306-315, 2008.
13. N. Kacem, S. Hentz, D. Pinto, B. Reig, and V. Nguyen, Nonlinear dynamics of nanomechanical beam resonators: Improving the performance of NEMS-based sensors. Nanotechnology, vol. 20, 275501, 2009.
14. N.C. Murgude and J.N. Reddy, Nonlinear analysis of microbeam under electrostatic loading, Mechanics of Advanced Materials and Structures, vol. 13, pp. 13-32, 2006.
15. J.H. Kuang and C.J. Chen, Dynamic characteristics of shaped micro-actuators solved using the differential quadrature method. Journal of Micromechanics and Microengineering, vol. 14, pp. 647-655, 2004.
16. M.H. Ghayesh, H. Farokhi, and M. Amabili, Nonlinear behavior of electrically actuated MEMS resonators. International Journal of Engineering Science, vol. 71, pp. 137-155, 2013.
17. F.M. Alsaleem, M.I. Younis, and H.M. Ouakad, On the nonlinear resonances and dynamic pull-in of electrostatically actuated resonators. Journal of Micromechanics and Microengineering, vol. 19, 045013, 2009.
18. M. Moghimi Zand, The dynamic pull-in instability and snap-through behavior of initially curved microbeams, Mechanics of Advanced Materials and Structures, vol. 19, pp. 485-491, 2012.
19. W.G. Dantas, and A. Gusso, Analysis of the chaotic dynamics of MEMS/NEMS doubly clamped beam resonators with two-sided electrodes. International Journal of Bifurcation and Chaos, vol. 28, 1850122, 2018.
20. M.I. Younis and A.H. Nayfeh, A study of the nonlinear response of a resonant microbeam to an electric actuation. Nonlinear Dynamics, vol. 31, pp. 91-117, 2003.
21. W.M. Zhang, and G. Meng, Nonlinear dynamic analysis of electrostatically actuated resonant MEMS sensors under parametric excitation. IEEE Sensors Journal, vol. 7, pp. 370-380, 2007.
22. A.M. Elshurafa, K. Khirallah, H.H. Tawfik, A. Emira, A.K.S. Abdel Aziz, and S.M. Sedky, Nonlinear dynamics of spring softening and hardening in folded-MEMS comb drive resonators. Journal of Microelectromechanical Systems, vol. 20, pp. 943-958, 2011.

23. G. Rezazadeh, H. Madinei, and R. Shabani, Study of parametric oscillation of an electrostatically actuated microbeam using variational iteration method. Applied Mathematical Modelling, vol. 36, pp. 430-443, 2012.
24. D.I. Caruntu and M. Knecht, On nonlinear response near-half natural frequency of electrostatically actuated microresonators. International Journal of Structural Stability and Dynamics, vol. 11, pp. 641-672, 2011.
25. D.I. Caruntu and K.N. Taylor, Bifurcation type change of AC electrostatically actuated MEMS resonators due to DC bias. Shock and Vibration, 542023, 2014.
26. Y.H. Qian, D.X. Ren, S.K. Lai, S.M. Chen, Analytical approximations to nonlinear vibration of an electrostatically actuated microbeam, Communications in Nonlinear Science and Numerical Simulation, vol. 17, pp. 1947-1955, 2012.
27. J.X. Han, Q.C. Zhang, and W. Wang, Design considerations on large amplitude vibration of a doubly clamped microresonator with two symmetrically located electrodes, Communications in Nonlinear Science and Numerical Simulation, 22, 492-510, 2015.
28. J.X. Han, Q.C. Zhang, and W. Wang, Static bifurcation and primary resonance analysis of a MEMS resonator actuated by two symmetrical electrodes. Nonlinear Dynamics, vol. 80, pp. 1585-1599, 2015.
29. L. Li and Q.C. Zhang, Nonlinear dynamic analysis of electrically actuated viscoelastic bi-stable microbeam system. Nonlinear Dynamics, vol. 87, pp. 587-604, 2017.
30. M. Saadatmand and A. Shooshtari, Nonlinear vibration analysis of a circular micro-plate in two-sided NEMS/MEMS capacitive system by using harmonic balance method, Acta Mechanica Sinica, doi.org/10.1007/s10409-018-0794-8, 2018.
31. B.S. Wu, W.P. Sun, and C.W. Lim, An analytical approximate technique for a class of strongly non-linear oscillators. International Journal of Non-Linear Mechanics, vol. 41, pp. 766-774, 2006.
32. W.P. Sun and B.S. Wu, Accurate analytical approximate solutions to general strong nonlinear oscillators. Nonlinear Dynamics, vol. 51, pp. 277-287, 2008.
33. D.F. Tang, C.W. Lim, L. Hong, J. Jiang, and S.K. Lai. Dynamic response and stability analysis with Newton harmonic balance method for nonlinear oscillating dielectric elastomer balloons, International Journal of Structural Stability and Dynamics, vol. 18, 1850152, 2018.

34. B.S. Wu and W.P. Sun, Construction of approximate analytical solutions to strongly nonlinear damped oscillators, Archive of Applied Mechanics, vol. 81, pp. 1017-1030, 2011.
35. B.S. Wu, Z. Yang, C.W. Lim, and W.P. Sun, Analytical approximations to resonance response of harmonically forced strongly odd nonlinear oscillators. Archive of Applied Mechanics, vol. 88, pp. 2123-2134, 2018.
36. B.S. Wu, W.J. Liu, X. Chen, and C.W. Lim, Asymptotic analysis and accurate approximate solutions for strongly nonlinear conservative symmetric oscillators. Applied Mathematical Modelling, vol. 49, pp. 243-254, 2017.
37. Y.P. Yu, B.S. Wu, and C.W. Lim, Numerical and analytical approximations to large post-buckling deformation of MEMS, International Journal of Mechanical Sciences, vol. 55, pp. 95-103, 2012.
38. Y.H. Sun and Y.P. Yu, Closed form solutions for the large post-buckling deformation of radio frequency-micro-electromechanical systems beams subjected to electrostatic loads, Journal of Computational and Theoretical Nanoscience, vol. 12, pp. 3044-3049, 2015.
39. W.J. Liu, B.S. Wu, and C.W. Lim, Linear and nonlinear free vibrations of electrostatically actuated micro-/nanomechanical resonators, Microsystem Technologies, vol. 23, pp. 113-123, 2017.
40. M. Moghimi and M.T. Ahmadian, Application of homotopy analysis method in studying dynamic pull-in instability of microsystems, Mechanics Research Communications, vol. 36, pp. 851-858, 2009.
41. B.S. Wu and C.W. Lim, Large amplitude non-linear oscillations of a general conservative system, International Journal of Non-Linear Mechanics, vol. 39, pp. 859-870, 2004.
42. A.H. Nayfeh and D.T. Mook, Nonlinear Oscillations, Wiley, 1995.

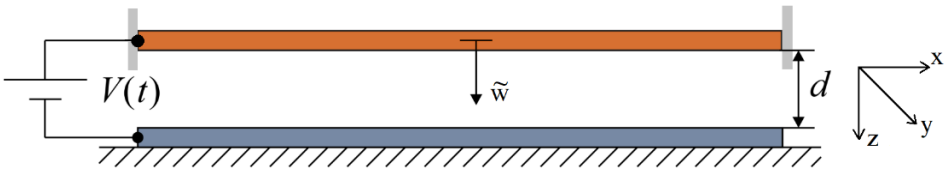

(a)

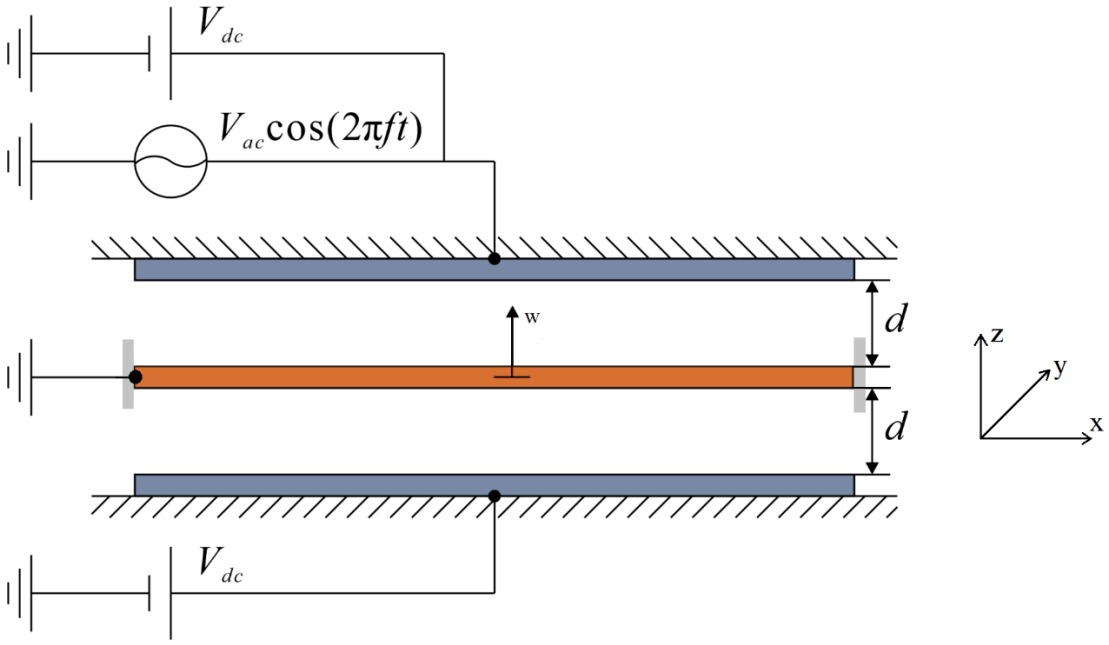

(b)

Fig. 1. (a) Schematic of a doubly-clamped microbeam actuated by one-sided electrode; (b) Schematic of a doubly-clamped microbeam driven by two-sided electrodes.

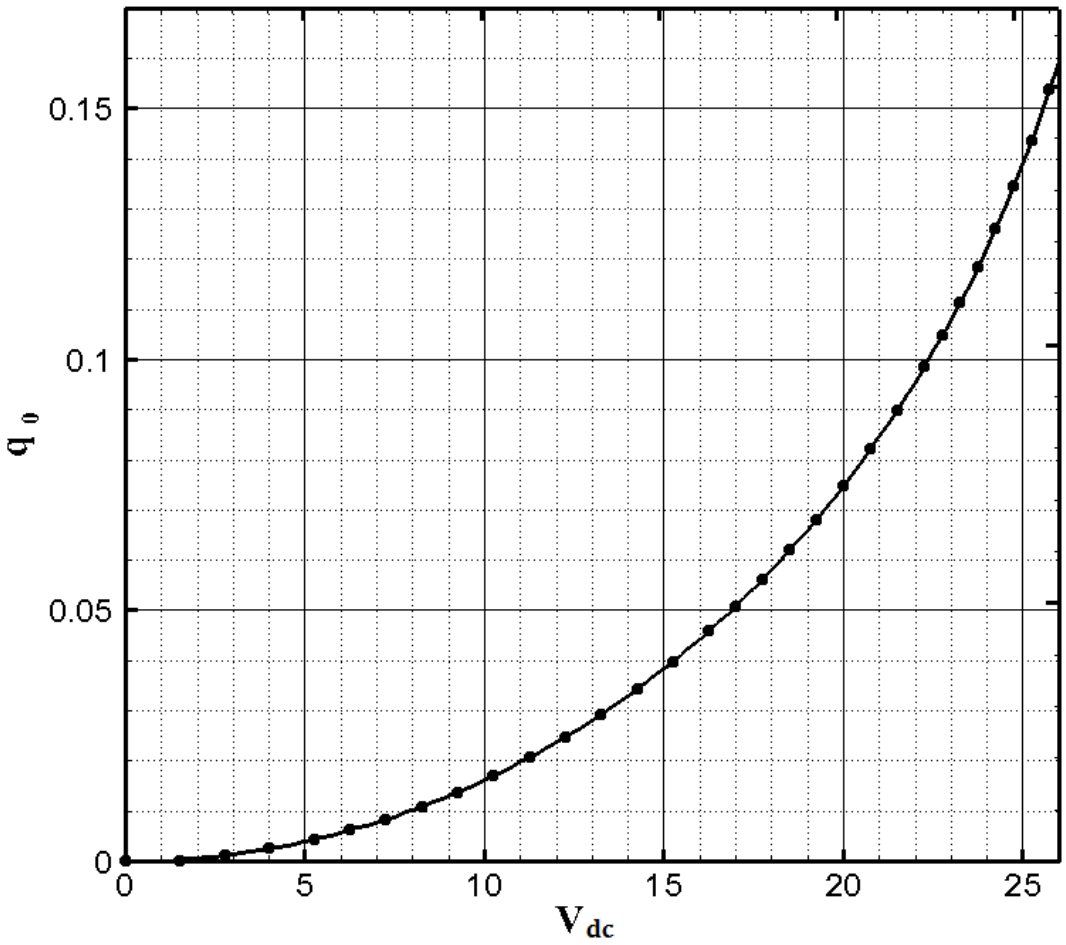

512

513 Fig. 2. Values of the equilibrium position q_0 for various electrostatic actuations V_{dc}

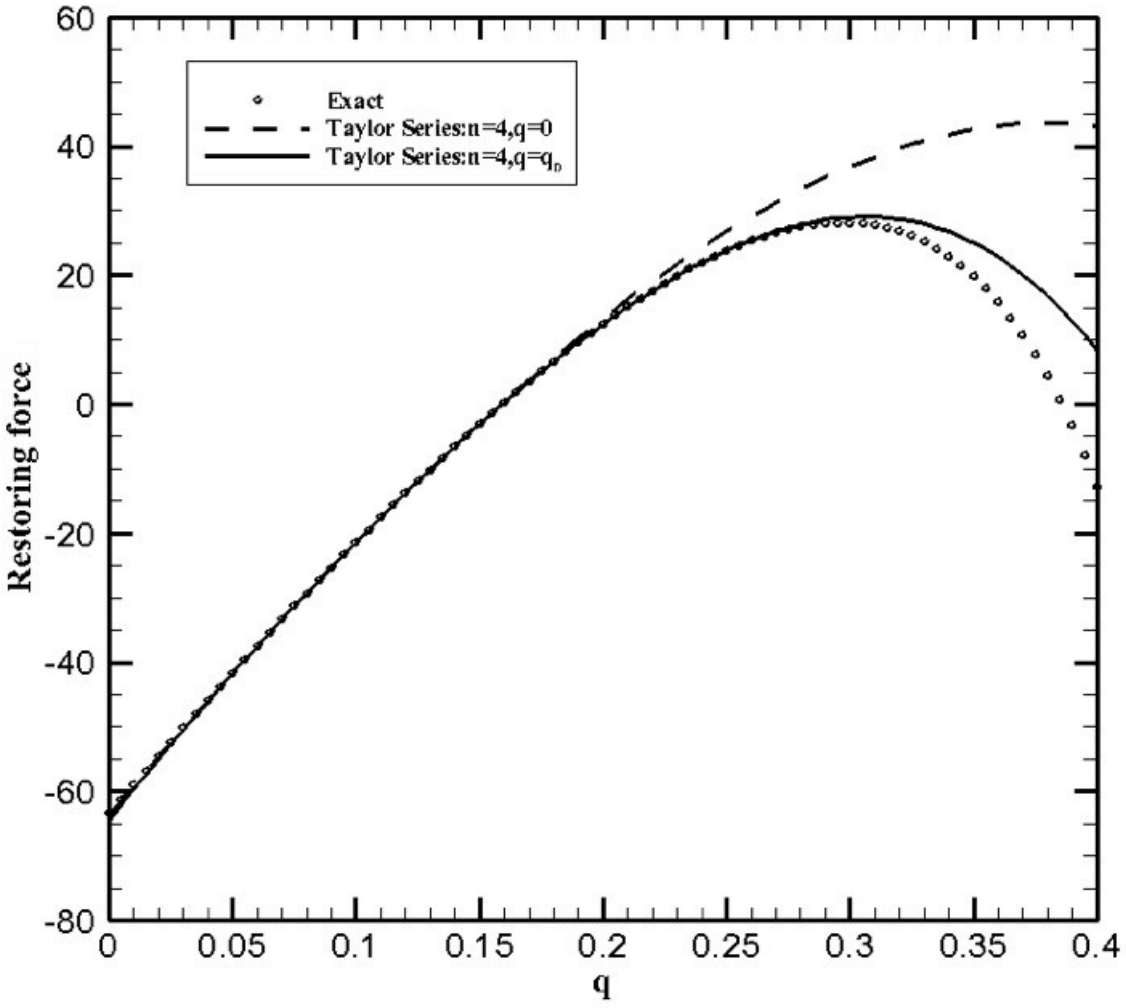

Fig. 3. Comparison of the restoring forces of three models under an input voltage 25V.

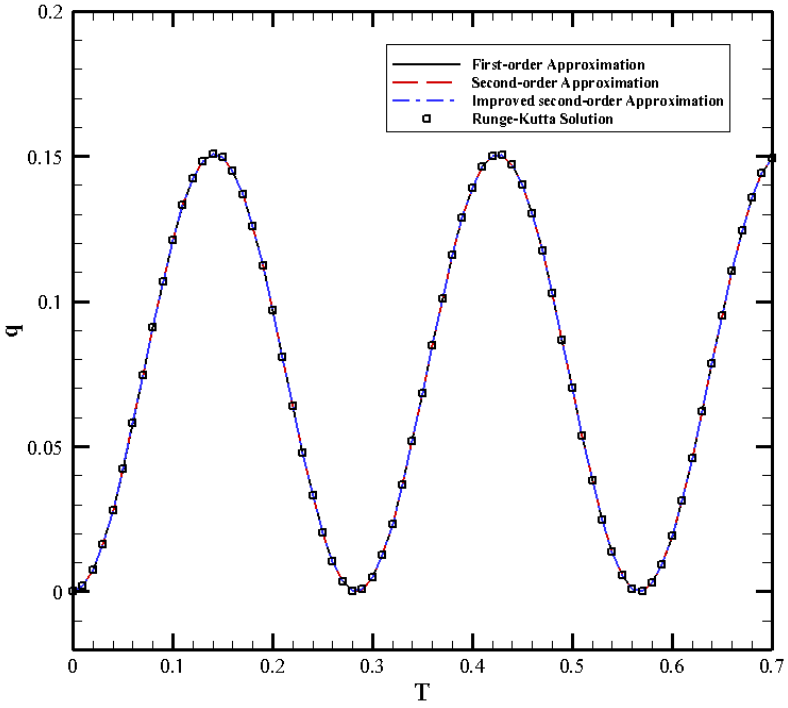

(a)

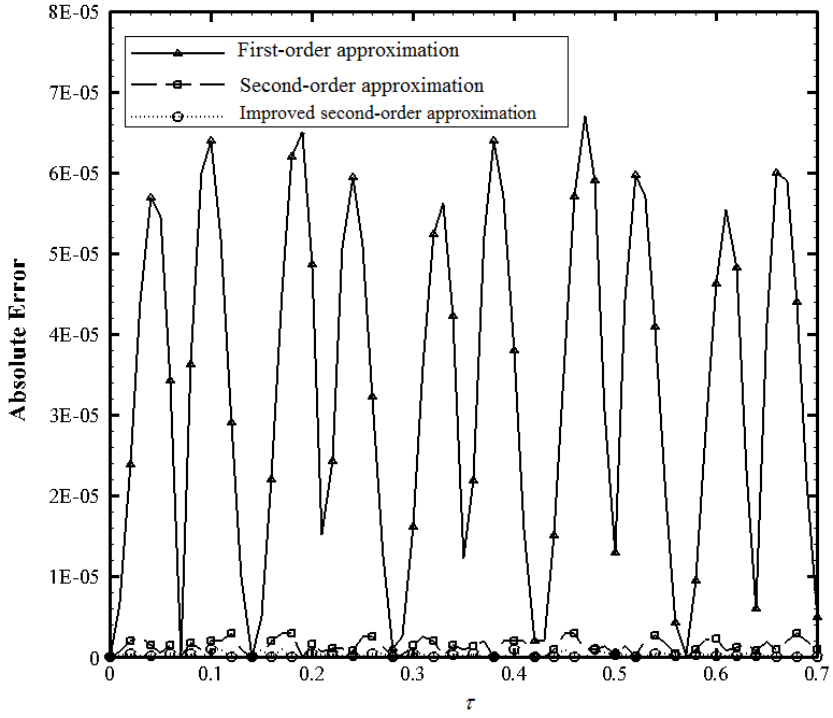

(b)

Fig. 4. (a) Time-history responses for the input voltage V_{dc} = 20V;
(b) Comparison of the absolute errors between the approximate and numerical solutions.

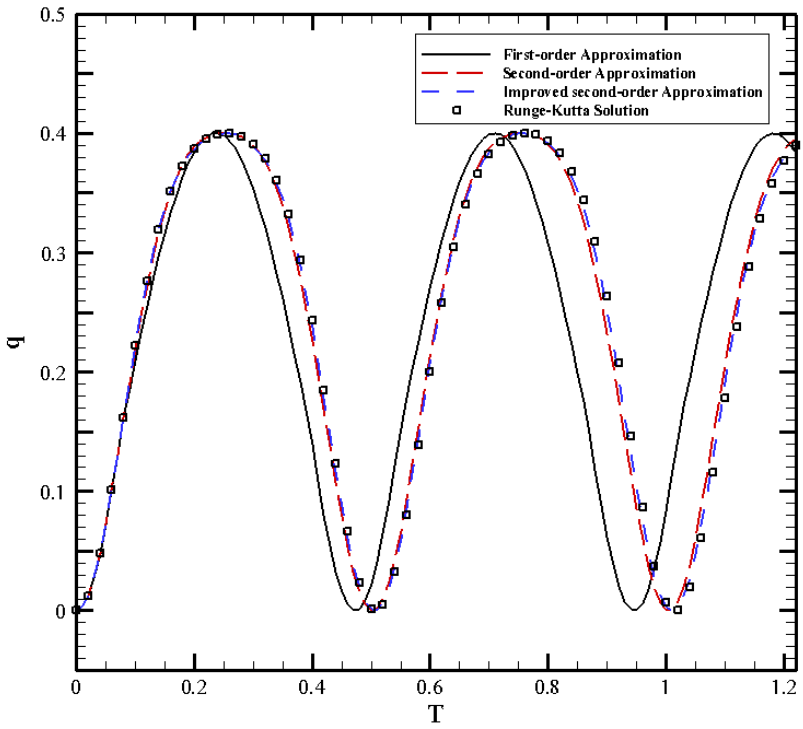

(a)

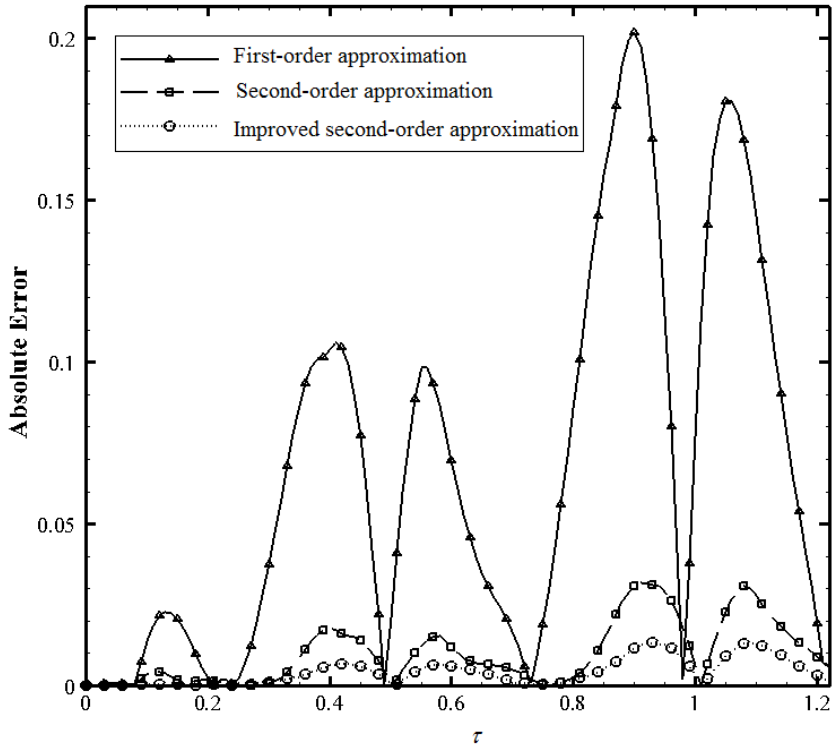

(b)

Fig. 5. (a) Time-history responses for the input voltage V_{dc} = 25.5 V; (b) Comparison of the absolute errors between the approximate and numerical solutions.

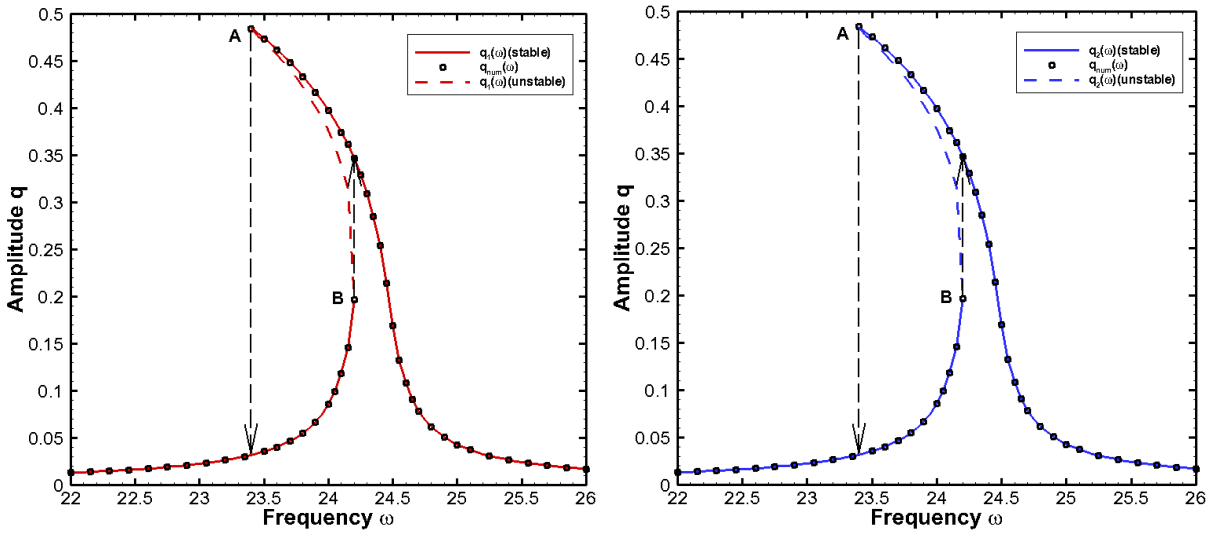

(a) (b)

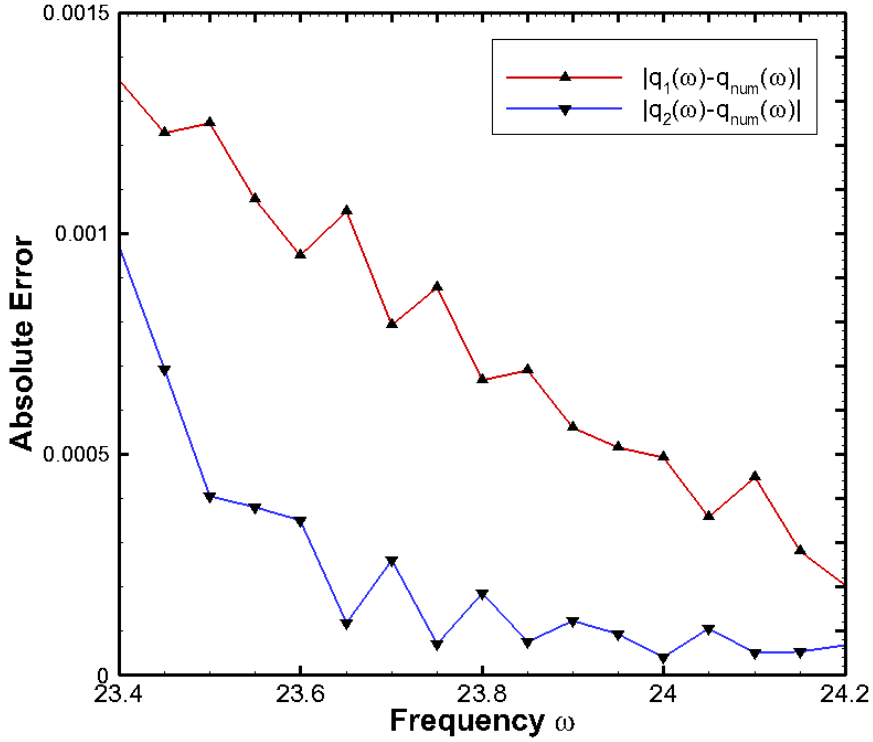

(c)

Fig. 6. (a) First-order analytical approximate frequency-amplitude response for V_{dc} = 8 V and V_{ac} = 0.2 V; (b) Second-order analytical approximate frequency-amplitude response for V_{dc} = 8 V and V_{ac} = 0.2 V; and (c) Comparison of the absolute errors between the approximate and numerical solutions.

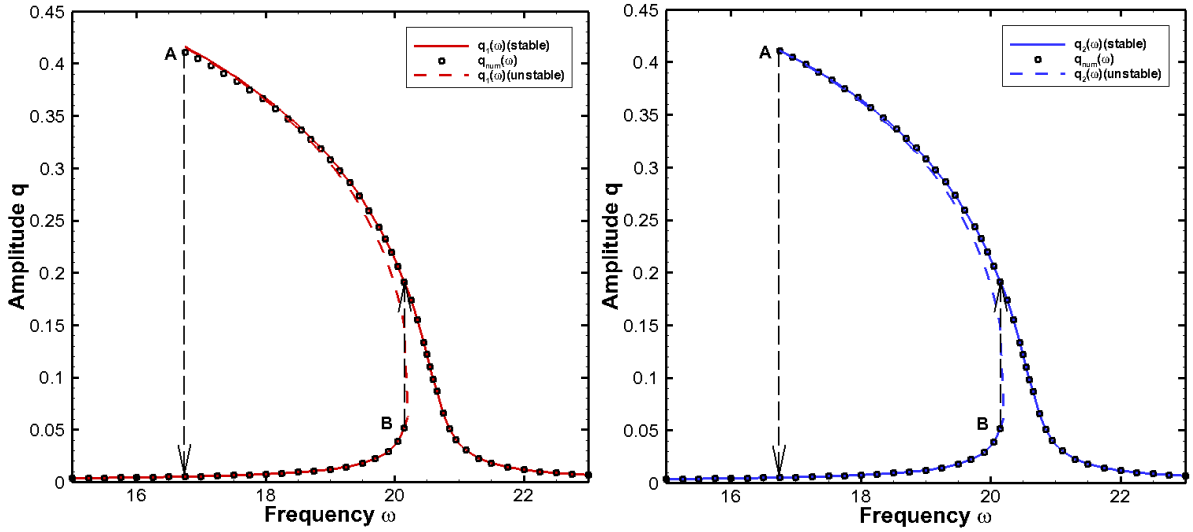

(a) (b)

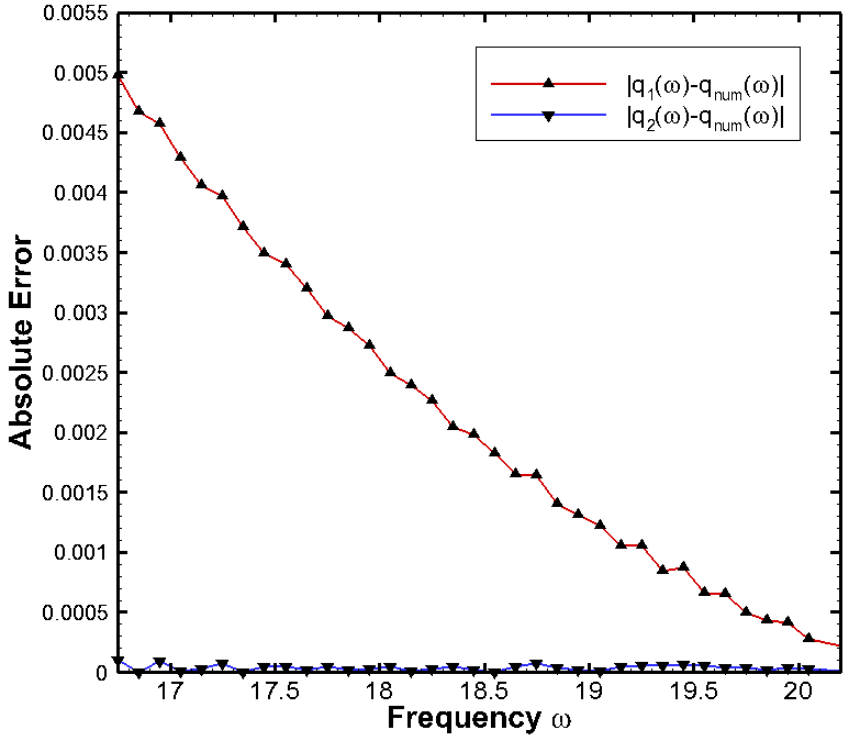

(c)

Fig. 7. (a) First-order analytical approximate frequency-amplitude response for V_{dc} = 12 V and V_{ac} = 0.07 V; (b) Second-order analytical approximate frequency-amplitude response for V_{dc} = 12 V and V_{ac} = 0.07 V; and (c) Comparison of the absolute errors between the approximate and numerical solutions.

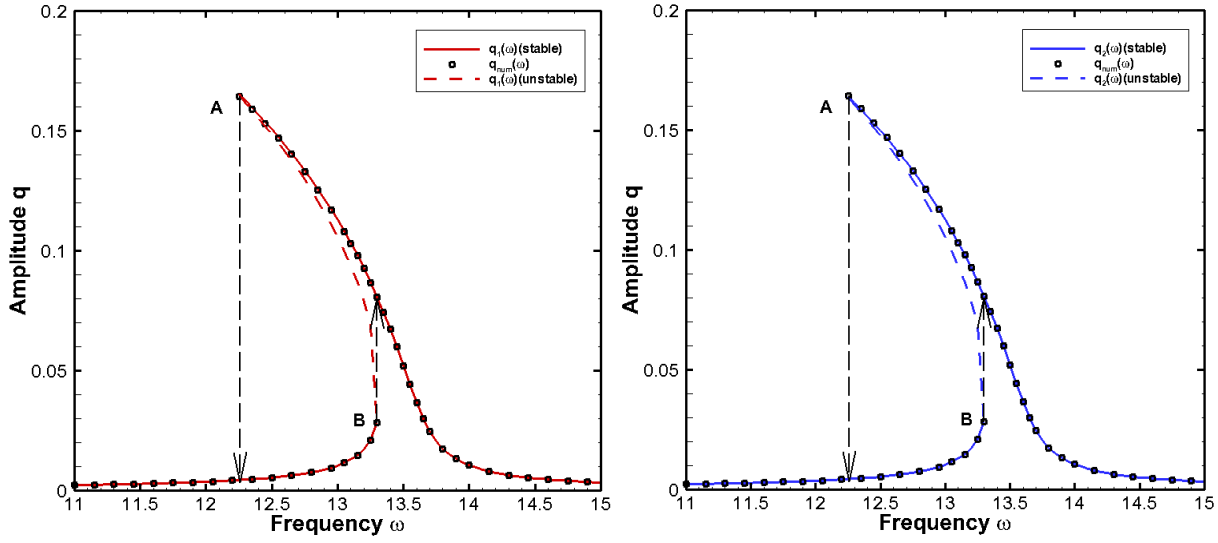

(a) (b)

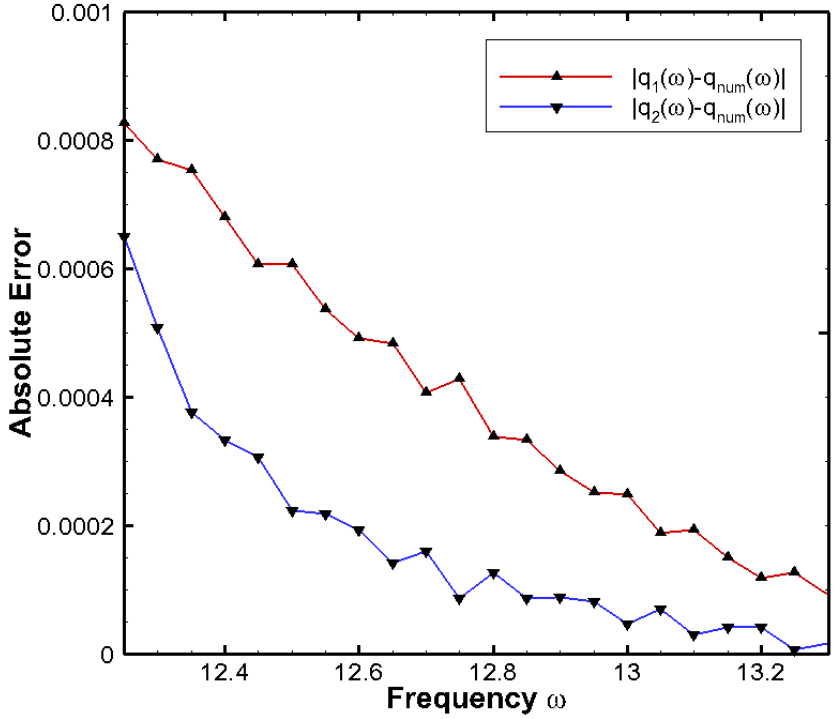

(c)

Fig. 8. (a) First-order analytical approximate frequency-amplitude response for V_{dc} = 16 V and V_{ac} = 0.01 V; (b) Second-order analytical approximate frequency-amplitude response for V_{dc} = 16 V and V_{ac} = 0.01 V ; and (c) Comparison of the absolute errors between the approximate and numerical solutions.

Table 1. Geometrical and material parameters of a MEMS microbeam[5,20,40]

Parameter	Symbol	Value
Length of beam	L	210 μm (for case 1*)
		310 μm (for case 2*)
Width of beam	b	100 μm
Thickness of beam	h	1.5 μm
Nominal gap	d	1.18 μm
Young's modulus	E'	151 GPa
Poisson's ratio	υ	0.3
Density of beam	ρ	2332 kg/m^3
Initial axial load	N_i	0.0009 N
Dielectric constant of the gap medium	ε_0	8.854×10^{-12} F/m
Quality factor	Q	197

*Cases 1 and 2 correspond to a doubly-clamped microbeam with one-side electrode and two-sided electrodes, respectively. Only the beam length is different, other parameters are the same in both cases.

559 Table 2. Values of DC dynamic pull-in voltage for different models

Length of beam (μm)	DC dynamic pull-in voltage (V)		
	Model 1 (Eq. 14)	Model 2 (Eq. 16)	Model 3 (Eq. 17)
210	25.84	26.96	26.02
310	12.94	13.46	13.03
410	8.18	8.49	8.23
510	5.87	6.08	5.90

560

561 Table 3. Equilibrium points and initial frequencies under various input voltage values

V_{dc} (V)	Equilibrium point	ω_1 (Eq. 55)	ω_2 (Eq. 57)	ω_2^* (Eq. 59)	ω_e (Eq. 79)
2	0.0006	24.5815	24.5815	24.5815	24.5815
8	0.0102	24.2969	24.2969	24.2969	24.2969
14	0.0330	23.5950	23.5950	23.5950	23.5950
20	0.0748	22.1461	22.1461	22.1461	22.1461
22	0.0955	21.2774	21.2770	21.2770	21.2770
24	0.1222	19.8367	19.8339	19.8430	19.8430
25	0.1389	18.4935	18.4806	18.4811	18.4810
26	0.1593	13.2852	12.5064	12.4346	12.3827

562